UNIVERSITY OF HELSINKI REPORT SERIES IN PHYSICS

HU-P-107

Modeling of high-dose radiation damage in semiconductors

Janne Nord

Accelerator Laboratory
Department of Physical Sciences
Faculty of Science
University of Helsinki
Helsinki, Finland

ACADEMIC DISSERTATION

To be presented, with the permission of the Faculty of Science of the University of Helsinki, for public criticism in the Small auditorium (E204) of Physicum, on November 22nd, 2003, at 10 o'clock a.m.

HELSINKI 2003

ISBN 952-10-0937-3 (printed version)
ISSN 0356-0961
Helsinki 2003
Yliopistopaino

ISBN 952-10-0938-1 (PDF version)
http://ethesis.helsinki.fi/
Helsinki 2003
Helsingin yliopiston verkkojulkaisut

J. Nord: **Modeling of high-dose radiation damage in semiconductors** University of Helsinki, 2003, 38 p.+appendices, University of Helsinki Report Series in Physics, HU-P-D107, ISSN 0356-0961, ISBN 952-10-0937-3

Classification (INSPEC): A3410
Keywords (INSPEC): Molecular dynamics method, ion implantation, radiation damage

ABSTRACT

The rapid development of electronic components places a huge demand on the improvements of processing methods. Novel and complex methods, such as ion beam implantation, are used in device production. To further develop the implantation techniques, it is necessary to understand the damage production during ion beam irradiation.

Some processes involved in damage production and recombination are difficult to study experimentally. The molecular dynamics (MD) method is a powerful tool for obtaining atomic level information on ion irradiation related phenomena in semiconductors, but the validity of the results depends strongly on the quality of the interatomic potential model. In this thesis a number of potential models for compound semiconductors are analyzed, and severe problems are found. New, accurate and transferable potential models are developed for Ga, As, N, GaAs and GaN systems. They are designed for the modeling of far-from-equilibrium effects, such as ion beam irradiation. The new interatomic potentials are applied to model irradiation effects in GaAs and GaN.

An iterative method for the simulation of high dose amorphization is described in this work. The method is applied to Si, Ge, GaAs and GaN. Si and Ge are important materials since they are widely used in the semiconductor industry, while GaAs and GaN are important for optoelectronic applications. The validity of the models, structural properties of the amorphous materials and the mechanisms leading to amorphization are discussed.

It was found that the low energy recoils (3 - 15 eV) can cause significant athermal recrystallization during ion beam irradiation of Si. Two reasons were found for the high irradiation dose needed to amorphize GaN: the high threshold displacement energy leading to low damage production in individual cascades, and the in-cascade recombination of defects. It was shown that the direct impact induced amorphous pockets explain the dependence of the damage level on the implantation angle in Er doped GaN.

2

CONTENTS

1 INTRODUCTION

The need for faster and smaller components creates a need to develop processing methods in semiconductors, which are the basis of modern electronics [1]. Ion implantation of dopants is an important method for semiconductor processing [2]. It allows for a good level of control of the dopant depths and profiles. However, ion beam implantation of semiconductors damages the material and leads to amorphization at high doses. Understanding the mechanisms leading to damage production and amorphization, as well as the quality of the damage, is necessary for the development of more accurate processing methods.

Silicon and germanium are two of the most commonly used semiconductor materials. Ion beam processes in them have been widely studied, but more research is needed for further miniaturization of components.

The implantation methods for GaAs and GaN are much less developed than for Si and Ge. For GaN especially the p-type doping has been a difficult problem[3]. Both GaN and GaAs are important for optoelectronic applications.

Due to the complexity of the amorphization process and the many-body effects involved, the problem can not be solved analytically. Experiments can provide valuable information about the results of implantation, but detailed 3D atomic level information is difficult to obtain. The short time scale dynamics of the processes in particular are difficult to study experimentally.

Atomic level understanding of the amorphization processes can be obtained by using computer simulations. For the present problem, a purely quantum mechanical approach is computationally too demanding for modern computers. The time and length scales in high dose irradiation effects are suitable for molecular dynamics (MD) methods. Since the accuracy of the MD simulations depends strongly on the quality of the interatomic potential models, special attention must be paid to the properties of the potential models.

2 PURPOSE AND STRUCTURE OF THIS STUDY

The purpose of this study is to improve the understanding of defect accumulation and amorphization processes in high dose irradiation in Si, Ge, GaAs and GaN.

This study consists of this preface and the following six articles published or accepted for publication in refereed international scientific journals. The articles will be referred to by Roman numbers in the text.

In the first article many existing interatomic potential models for compound semiconductors are found unsuitable for modeling high dose ion irradiation phenomena. Hence, new interatomic potential models are presented for GaAs and GaN, in papers II and III, respectively. The results of the simulations of high dose irradiation of Si, Ge and GaAs are presented in paper IV and and GaN in paper V. The role of the implantation angle on the damage production in GaN is discussed in paper VI.

Summaries of the original papers

Paper I: Strain-induced Kirkendall mixing at semiconductor interfaces, K. Nordlund, J. Nord, J. Frantz and J. Keinonen, *Comput. Mater. Sci.* **18**, (2000) 283-294.

In this paper the effects of the interface between different semiconductor materials on the damage production during ion beam irradiation are studied. The properties of interatomic potential models for compound semiconductors are analyzed and problems are found with many of them. The limitations of the properties of the potential models for compound semiconductors motivated the development of new models.

Paper II: Modelling of compound semiconductors: Analytical bond-order potential for Ga, As, and GaAs, K. Albe, K. Nordlund, J. Nord and A. Kuronen, *Phys. Rev. B* **66**, 035205 (2002).

A new interatomic potential model for Ga, As and GaAs is presented. Special emphasis is placed on the description of the pure constituents and different coordinations. Melting point, elastic constants and defect properties are reasonably well described by the model. This makes the model well suited to study irradiation effects.

Paper III: Modelling of compound semiconductors: Analytical bond-order potential for gallium, nitrogen and gallium nitride, J. Nord, K Albe, P Erhart and K Nordlund, *J. Phys.: Condens. Matter* **15**, 5649-5662 (2003).

In this work an interatomic potential model for Ga, N, and GaN is presented. The analytical model describes a wide range of structural properties of the materials. The melting point, defect formation energies, solubility of atomic nitrogen in liquid gallium and elastic constants are reasonably described by the model. The model is therefore well suited to study the irradiation effects.

Paper IV: Amorphization mechanism and defect structures in ion-beam-amorphized Si, Ge, and GaAs, J. Nord, K. Nordlund and J. Keinonen, *Phys Rev. B* **65**, 165329 (2002).

Ion beam induced amorphization in Si, Ge and GaAs is modeled in this paper. Three different interatomic potential models are used for Si and two for Ge. In this way the dependency of the results on the potential model can be estimated. The results are compared to experimental observations and good agreement is found with them for many properties. It is found that the low energy recoils (3 - 15 eV) can cause significant athermal recrystallization during irradiation and that the amorphization of Si proceeds predominantly by the growth of amorphous pockets. The structural properties of amorphous materials are discussed.

Paper V: A molecular dynamics study of damage accumulation in GaN during ion beam irradiation, J. Nord, K. Nordlund and J. Keinonen, *Phys. Rev. B*, accepted for publication

In this work the damage produced by ion beam bombardment of GaN is modeled. Both individual recoils and damage accumulation caused by successive recoils are studied. Nitrogen gas is found for be produced during irradiation. Two reasons are found to the high amorphization dose of GaN: the high threshold displacement energy leading to low damage production in individual cascades and in-cascade recombination of defects.

Paper VI: Implantation angle dependence of ion irradiation damage in GaN, J. Nord, K. Nordlund, J. Keinonen, B. Pipeleers and A. Vantomme, *Materials Science and Engineering B*, accepted for publication

The dependence of the damage on the implantation angle is studied in this paper. The simulation model reproduces the experimentally observed angular behavior. It is found that for small angles there is less damage and the damage is more scattered than for larger angles, and that direct impact induced amorphous pockets explain the behavior observed in the experiments.

Author's contribution

The publications presented in this thesis are a result of group work. In paper I the author performed the simulations and testing of potential models for compound semiconductors and fitted the InAs parameters. The testing of the properties of Ga, As, N, GaAs and GaN potential models in papers II and III were performed by the author, who also fitted the parameters for Ga-N and refined (especially the cutoff values) the other parameterizations in these papers. The testing of surface properties in paper II and the solubility simulations in paper III were performed by co-authors, and the additional quantum mechanical calculations were performed by K. Albe.

All the simulations in papers IV-VI were performed by the author, who also wrote the majority of papers IV-VI and participated in writing the papers I-III.

The functional form of the ionic potential model presented in section 4.5 was developed by Karsten Albe. The simulation results for the ionic model presented in this thesis are calculated by the author, who also fitted the parameters of the covalent part of the long range GaN potential model.

3 MODELS FOR DAMAGE ACCUMULATION DURING IRRADIATION

3.1 Analytical models

There are several empirical analytical models describing the development of the damage level in the material during irradiation [4–9]. The damage level is described by the amorphous fraction, which is the level of damage compared to fully amorphized material. In these models the functional form is derived from an assumed damage accumulation mechanism. The functional form has free parameters, which are fitted to reproduce the experimentally observed development of the damage level during ion irradiation. The validity of the model can be estimated by how well the model can predict the changes in the development of the damage level when the irradiation conditions are varied.

The amorphization can proceed either homogeneously or heterogeneously. An illustration of these mechanisms is given in Fig.1. In a homogeneous process, point defects or specific defect types accumulate homogeneously throughout the volume. After a certain critical threshold level has been reached, the amorphization may occur spontaneously.

Damage is unevenly distributed in the heterogeneous amorphization process. Several mechanisms have been proposed for heterogeneous damage accumulation. In the direct impact amorphization mechanism, individual collision cascades produce damage that is frozen in. Another mechanism is the local accumulation of high defect concentrations due to overlapping cascades. In the defect-stimulated model amorphization is assumed to proceed via nucleation and growth processes. Examples of the development of amorphous fraction as described by different models are shown in Fig. 2.

In general, high mass and low energy ions produce dense localized defect regions, and heterogeneous amorphization occurs. High energy and light ions produce lower density defect regions, and may therefore induce homogeneous amorphization.

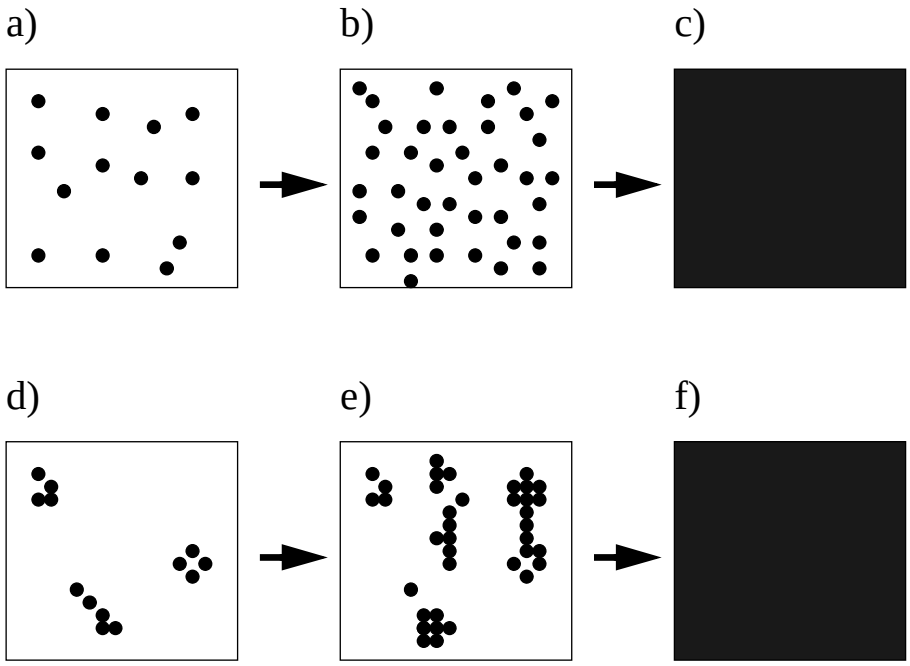

Figure 1: Illustration of Homogeneous (a-c) and heterogeneous (d-f) amorphization processes. In the homogeneous model the damage is evenly distributed in the material. In the heterogeneous model the damage is more concentrated.

None of the above models alone can describe the damage accumulation in all materials. Even in specific materials, the mechanisms may vary with irradiation conditions and parameters, and a combination of several mechanisms is needed to explain the observed behavior. Sometimes many models can produce good fits to the available data, and no definite judgment can be made on the underlying mechanisms. Hence computer simulations are a useful tool for studying the amorphization.

3.2 Binary collision approximation computer simulations

Binary collision approximation (BCA) methods [10] can be used to simulate the high dose irradiation of semiconductors [11, 12]. In this approach, the trajectories of the bombarding ions are calculated assuming that the atom collisions are separated and only two atoms are contributing to each collision. The trajectories of recoil atoms knocked by the bombardment ion can be included in the model.

The model can predict accurately the depth profile of deposited energy and the production of interstitials and vacancies in the high energy range. Since BCA simulations are computationally less demanding than molecular dynamics simulations (see section 3.3), higher irradiation doses and ener-

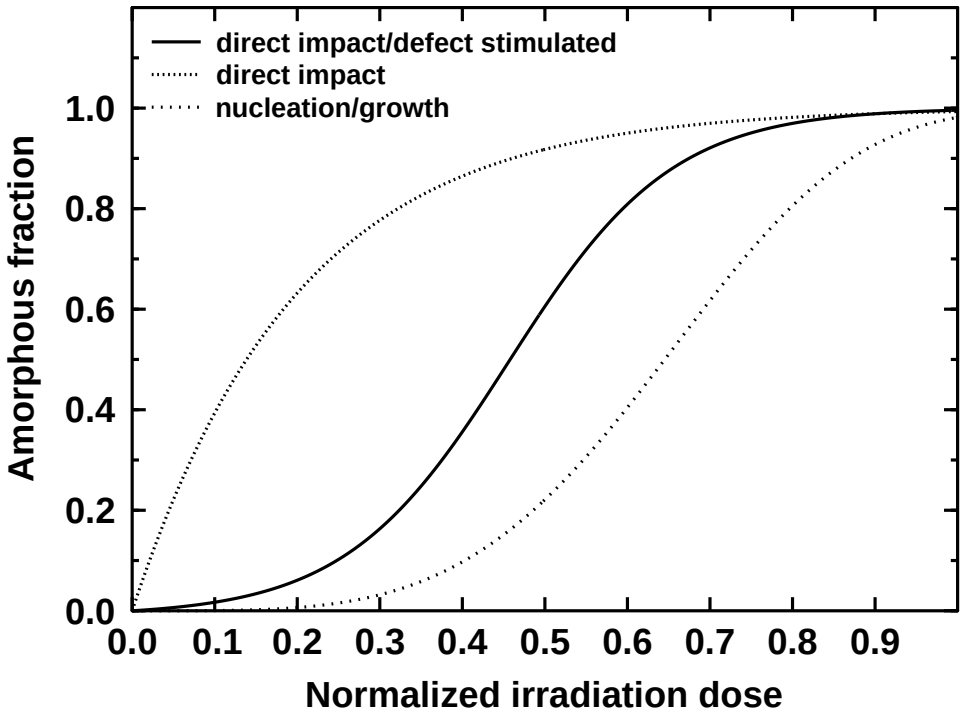

Figure 2: Amorphous fraction as a function of normalized irradiation dose for different empirical analytical models.

gies can be simulated. The migration and recombination of point defects can further be simulated by using kinetic Monte Carlo methods [12].

The use of the BCA method to simulate amorphization processes has several drawbacks. First, the neglect of collisions with more than two contributing atoms at a time affects the trajectories of the ions at low energies. Since much of the damage is produced in the low energy range, the damage distribution is distorted. The second drawback is that BCA is not suitable for simulating liquid-like zones, which are important for the clustering of defects and the amorphization process. Third, BCA does not give the real atomic structure of the amorphous material or the intermediate states. Fourth, the contributing mechanisms have to be known in advance when using kinetic Monte Carlo simulations.

Modeling of damage accumulation can be used in BCA simulations to improve the range profiles of dopants in semiconductors [13–15]. However, it is not suitable for modeling the atomic level structure of ion beam amorphized semiconductors or the intermediate states before amorphization.

3.3 Molecular dynamics simulations

In classical molecular dynamics simulations Newton's equations of motion are solved iteratively for each atom. The forces between atoms are calculated using analytical interatomic potential models. Since the properties of the interatomic potential models play a crucial role in the validity of the results, careful attention has to be paid to them. Some of the potential models and the requirements for potentials used in the modeling of irradiation phenomena will be discussed in more detail in section 4.

Molecular dynamics methods have been widely used to study individual cascades and other irradiation processes in semiconductors, since the time and length scales in these phenomena are suitable for MD. Classical molecular dynamics allows the use of larger simulation cells and longer time scales than quantum mechanical approaches do. Systems consisting of millions of atoms can be simulated using MD and nanosecond time scales can be reached for smaller systems, whereas quantum mechanical approaches are limited to system sizes of about hundred atoms. The atomic level structure of the final and intermediate states can be extracted using this method, unlike in BCA. Finally, activation energies of atomic level processes, which are required for kinetic Monte Carlo simulations, are not needed in MD.

Several simulation methods have been used to model high dose irradiation effects in semiconductors [16–21]. The approach used in articles IV and V is explained below.

A schematic illustration of the simulation method is shown in Fig. 3. Initially the simulation cell contains perfect crystalline lattice. The cell is relaxed to zero pressure and the atoms have no kinetic energy. The size of the cell is selected so that the recoils initiated in the center are contained in the cell without crossing the borders. Periodic boundary conditions are used in all directions.

The simulations consist of two phases. In the first phase a recoil is simulated, and in the second phase the cell is relaxed and prepared for the next recoil. These two subsequent phases are iterated until full amorphization is observed. The damage level can be estimated by the changes in volume of the cell and the average potential energy of the atoms. When these two values have saturated, at least a nearly amorphous level has been reached. The two main phases are discussed in more detail below.

In the first phase, the recoil phase, an energetic recoil is initiated in the middle of the simulation cell. Throughout this phase, excess energy is removed using Berendsen temperature control [22] applied to the border atoms to cool the cell towards a temperature of 0 K. The cooling dampens the pressure waves before they re-enter the simulation cell from the opposite side and simulates the transfer of kinetic energy to the surrounding material.

In the second phase, the cell is relaxed to zero pressure and cooled efficiently toward 0 K using Berendsen methods [22]. The cooling is applied to all atoms in this phase. After the relaxation the atoms are displaced by a random vector, and moved back inside the simulation cell by applying periodic boundary conditions. Now the cell is ready for the next recoil.

The recoil energy is chosen as a representative recoil energy value for the modeled irradiation conditions. Recoil energies are higher for heavier than for lighter ions. 50 eV recoils have been used to model 1 MeV electron irradiation in Si using a fairly similar simulation method [17]. The most accurate description of the amorphization process can be obtained by using a simulated recoil energy distribution. Even in the case of simulated recoil energy distributions the lower and higher energy cutoff values must be chosen. Very low energy recoils (less than 10 eV) produce no or very little damage. The use of too low energy recoils increases the computational demands of the simulation but may give no additional information. A similar situation is posed by the high energy cutoff value. The minimum size of the simulation cell increases as the high energy cutoff value is increased. However, the high energy recoils break up into subcascades, which can be modeled by separate lower energy recoils.

Usually the initial direction of the recoils is chosen randomly. When simulating materials for which channeling effects are important, a more realistic description might be obtained by using a simulated angular distribution for initial recoil directions. The energy and direction distributions of recoil atoms can be simulated by using computationally less demanding approaches, such as BCA [10] or MDRANGE [23]. It should be noted that the accumulating damage changes both of these distributions.

The method described in this section can be used to generate continuous and homogeneous amorphous structures. It gives the atomic structures of amorphous and intermediate stages and the mechanisms involved in the amorphization process. The drawback of the method is that the long timescale defect migration processes are not reproduced, so the results are directly applicable only to low temperature (typically less than 100 K) irradiation conditions.

4 INTERATOMIC POTENTIAL MODELS

Interatomic potential models are simple energy functions that attempt to model the forces between atoms. They are needed when knowledge of the atomic level is required, but the time or length scale requirements exceed the available computer resources needed for quantum mechanical calculations.

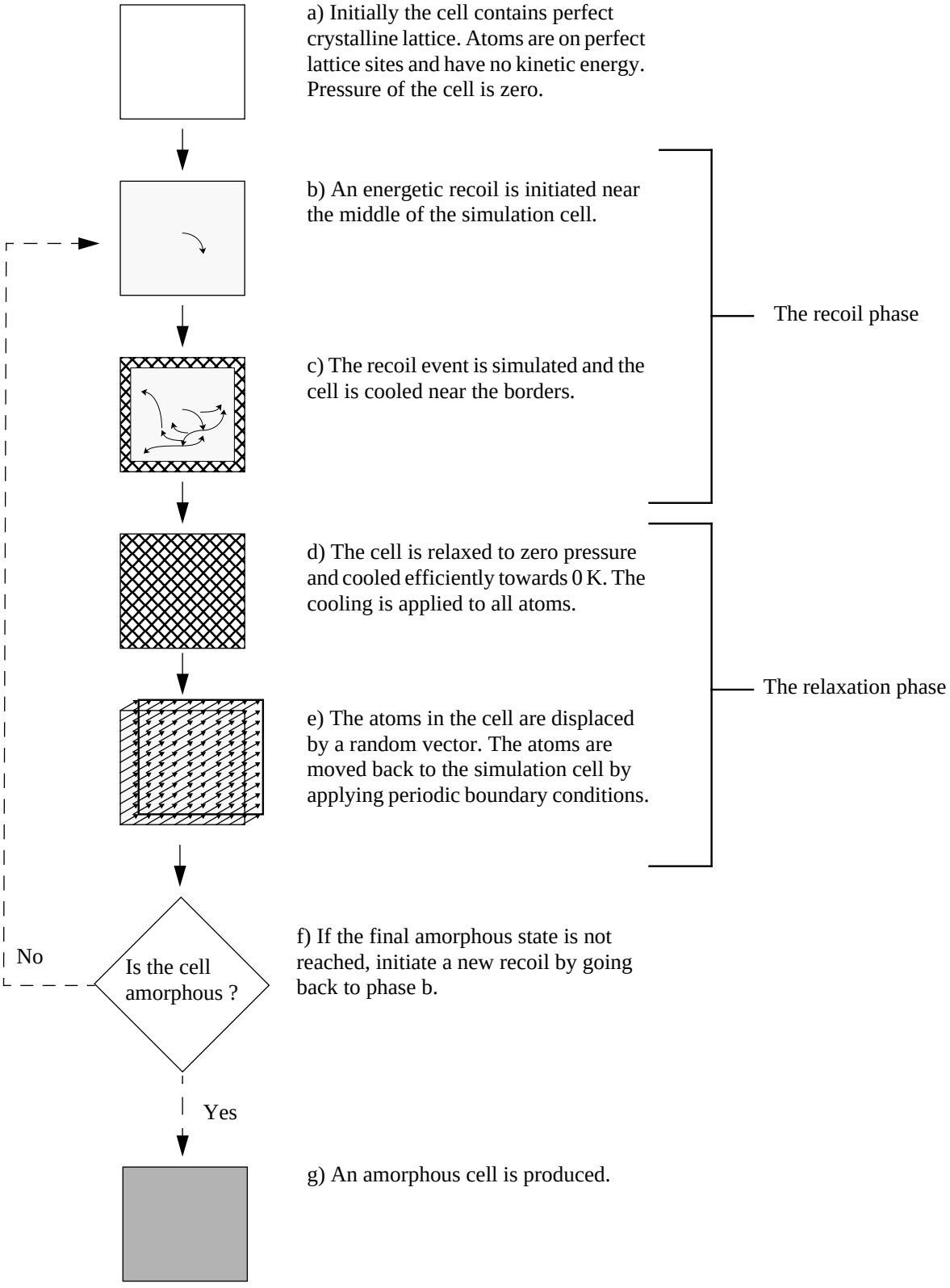

Figure 3: Method for creating amorphous cells using molecular dynamics simulations.

Many different functional forms have been proposed for analytical interatomic potential models even when the same materials are involved. On the other hand, close relationships between functional forms, which initially seem very different, have been pointed out [24, 25]. The potential models contain many parameters that are fitted to reproduce different sets of properties of the material. Again, a great variety of parameter sets is available for certain materials. Since the simulated behavior of the material is greatly affected by the potential model, the validity of the results also depends on the quality of the model. Therefore, careful attention must be paid to the suitability of the interatomic potential to model the problem at hand.

4.1 Requirements for the present problem

When an energetic ion travels through the target material, it loses some of its energy to recoil atoms. Dense collision cascades with a high energy density, molten zones, individual point defects, as well as high stress and strain states may be produced.

Since point defects are produced during ion beam irradiation, the potential model should reproduce point defect formation energies and geometries. The formation energies for defects may be obtained by quantum mechanical methods. Sometimes the literature data varies greatly, but at least the qualitative trends should be reproduced.

Melting behavior is an important property when simulating ion beam irradiation, since molten zones may be produced. Usually the melting point is not included in the systematic fitting of the parameters of the potential model, since relatively long simulations are needed to obtain it. Since melting point is often an experimentally well known property of a material, it provides a good test for the validity of the model.

Since strain and stress affect the outcome of the irradiation process, it is important that the potential reproduces the elastic constants. The elastic constants and lattice parameter are often included in the set of fitted parameters.

For compound semiconductors the properties of the pure constituents have to be reproduced as well. The compound nature of the material has an important role in the energetics of the disordered structures. For example, the number of odd rings may be limited due to the energy associated with the formation of like atom bonds [26]. Segregation of compounds is also possible in a liquid zone or during prolonged irradiation.

During irradiation, especially in molten zones, highly disordered configurations are formed. Therefore it is important that the potential reproduces the energetics of various configurations with different

coordination numbers. It is especially important that the correct ground state structure is reproduced. If the most stable structure is something else than the ground state structure of the natural material, the liquid zones may recrystallize in a wrong configuration and some defects will have a negative formation energy and will therefore be more stable than the perfect crystal.

4.2 Present models

In this section a short summary of the interatomic potential models for Si, Ge, GaAs and GaN is given.

Numerous interatomic potential models for silicon exist and have been extensively tested [27]. Tersoff potentials [28, 29], the Stillinger-Weber potential [30] and the more recent EDIP potential [31, 32] can be used to model irradiation effects.

The Tersoff [33] and Stillinger-Weber [34] potential models can describe the disordered phases of germanium. A modified version of the Stillinger-Weber parametrization, which lowers the melting point by changing the cohesive energy, was later used to model collision cascades [35].

All the potential models listed above for silicon and germanium give a good description of cubic elastic constants. The Stillinger-Weber potentials also have good melting properties. Since there are many models for Si and Ge, the risks for being mislead by artificial potential-related effects can be reduced by using several different potentials to model the phenomena.

For compound semiconductors, the situation is much less developed. A GaAs potential model based on the Tersoff formalism was proposed by Smith [36], but both pure constituents, Ga and As, have the wrong ground state structure in this model. Moreover, due to the weak angular term in the potential, the Young's modulus of zinc blende GaAs is very small, which leads to unrealistic deformations during irradiation. The Ga-As interaction parameters were later modified by Sayed *et al.*[37]. Since the parameters for pure constituents were not modified, gallium and arsenic still had the wrong ground states. The Sayed Ga-As parametrization gives a good description of elastic constants, but does not reproduce the correct ground state structure [38]. However, this problem can be corrected by modifying one of the parameter values, as done in paper I, in which a more detailed description of testing the GaAs potentials is also given.

Ito, Khor and Das Sarma [39] have proposed a different formalism to describe atomic interactions in GaAs. Since the parameter values for Ga-Ga and As-As interaction are not given, pure constituents are not described by this model. Therefore, the model can not be used to simulate ion beam irradiation in

GaAs. A potential based on the Stillinger-Weber formalism proposed by Ichimura [40] has the same problem.

Conrad and Scheerschmidt [41] have proposed a model for GaAs with parameters directly derived from tight binding momentum approximation. The model predicts a positive heat of formation for zinc blende GaAs, which leads to phase decomposition after heating and cooling [I].

A two-body potential model for GaN was presented by Zapol *et al.*[42]. The model reproduces wurtzite, zinc blende and rock salt structures. Wang *et al.*[43] have proposed a combination of Coulomb and Keating potentials, in which angularity was explicitly included. A Stillinger-Weber based potential was proposed by Aïchoune *et al.*[44]. Structural properties of pure constituents are not considered in any of the GaN potentials mentioned.

None of the above models for GaAs or GaN can describe pure gallium, arsenic or nitrogen. Therefore the models are not suitable for simulating highly disordered structures such as liquids, but can be used to model systems near the equilibrium structure. New interatomic potential models for GaN and GaAs, which can describe the properties of pure constituents, are presented in papers II and III and described briefly in sections 4.3 and 4.4.

4.3 Choosing the functional form

An interatomic potential model consists of the functional form and the parameter set. The functional form should allow the fitting of a wide range of materials properties, such as cohesive energies for different coordinations, lattice constants and elastic properties. To allow the fitting of many properties, many parameters are needed. On the other hand, the functional form should be physically well motivated. Potentials with a good physical basis, such as quantum mechanical bonding principles, are often more transferable than *ad hoc* potentials using more arbitrary functional forms [45]. A potential should also be accurate, in that it accurately reproduces the fitting database, and computationally is efficient.

An example of a functional form for interatomic potential models is briefly described here. The bond order formalism was originally introduced by Abell [46] and a practical implementation was later developed by Tersoff [29, 33]. A slightly modified version used here and in papers II and III for the GaAs and GaN potential models was proposed by Albe *et al.*[47]. The bond order formalism is chosen, because it can be used to describe several different structures, for example dimers, tetrahedral, bcc and fcc.

The total potential energy is written as a sum over individual bond energies:

$$E = \sum_i \sum_{i<j} f_{\mathrm{C}}(r_{ij})(V_{\mathrm{R}}(r_{ij}) - \frac{B_{ij}+B_{ji}}{2} V_{\mathrm{A}}(r_{ij})). \tag{1}$$

The cut-off function f_{C} can be chosen as

$$f_{\mathrm{C}}(r) = \begin{cases} 1, & \mathrm{r} \leqslant \mathrm{R\text{-}D} \\ \frac{1}{2} - \frac{1}{2}\sin\left[\pi \frac{(r-R)}{2D}\right], & R-D < r \leqslant R+D \\ 0, & \mathrm{r} \geqslant \mathrm{R{+}D}. \end{cases} \tag{2}$$

Here R is the cut-off distance and D is the range for which the cut is performed. R is often chosen between the nearest-neighbor and second-nearest neighbor distances. The pair-like repulsive and attractive parts are chosen to have Morse-like exponential forms,

$$V_{\mathrm{R}}(r) = Ae^{\lambda_1(r-r\mathrm{e})}, \tag{3}$$

$$V_{\mathrm{A}}(r) = Be^{\lambda_2(r-r\mathrm{e})}, \tag{4}$$

because this form allows easy fitting of dimer properties and bond-order dependency. Also the atomic orbitals are known to decay exponentially [46]. The bond order term

$$B_{ij} = (1+\xi_{ij})^{-1/2} \tag{5}$$

$$\xi_{ij} = \sum_{k(\neq i,j)} f_{ik}(r_{ik}) g_{ijk}(\theta_{ijk}) \exp(2\mu_{ik}(r_{ij}-r_{ik})) \tag{6}$$

and the pair-like terms of the functional form can be derived from a tight binding approach [47]. By choosing

$$A = \frac{D_0}{S-1}, \tag{7}$$

$$B = \frac{SD_0}{S-1}, \tag{8}$$

$$\lambda_1 = -\beta\sqrt{2S}, \tag{9}$$

and

$$\lambda_2 = -\beta\sqrt{2/S} \tag{10}$$

the binding energy of a dimer is D_0 and the dimer separation is r_e. If the ground state frequency of the dimer molecule is known, the β parameter is given by

$$\beta = \frac{k2\pi c}{\sqrt{2D_0\mu}}, \tag{11}$$

where k is the wave number for the ground state vibration frequency and μ the reduced mass. The parameter S is determined by the equilibrium bonding distance r_b and the energy-bond relation E_b of different structures,

$$E_b = -D_0 \exp(-\beta\sqrt{2S}(r_b - r_e)). \tag{12}$$

The choice of the angular part is more arbitrary, and many formalisms have been proposed [24]. In the GaAs and GaN potentials presented in papers II and III the form

$$g_{ijk}(\theta_{ijk}) = \gamma\Big(1 + \frac{c^2}{d^2} - \frac{c^2}{(d^2 + (h + \cos\theta_{ijk})^2}\Big) \tag{13}$$

has been chosen.

4.4 Fitting the parameters

After the functional form of the potential model has been chosen, the parameters are fitted. In this section the properties of Ga-Ga, As-As, N-N, Ga-As and Ga-N interactions presented in papers II and III are shortly described. The functional form given in section 4.3 is used.

The interactions were fitted independently and the properties that were affected by the interplay of the models, such as melting, were analyzed later. The initial parameters for the pair-like terms were first selected to reproduce the slope of energy-bond relation, bulk modulus and the dimer properties. Finally the other elastic constants and structural properties were fitted simultaneously using the Levenberg-Marquardt method [48].

The melting points for different components were simulated by using a liquid-solid equilibrium method [49]. In this technique, coexisting liquid and solid phases are simulated at different temperatures until crystallization or melting is observed. The simulations also serve as a test of the ground state structure.

The final parameters of the potential models are shown in table 1.

ij	Ga-Ga	N-N	As-As	Ga-N	Ga-As
γ	0.007874	0.76612	0.455	0.001632	0.0166
S	1.11	1.4922	1.86	1.1122	1.1417
$\beta(\text{Å}^{-1})$	1.08	2.05945	1.435	1.968	1.5228
D_e(eV)	1.40	9.91	3.96	2.45	2.10
R_e (Å)	2.3235	1.11	2.1	1.921	2.35
c	1.918	0.178493	0.1186	65.207	1.29
d	0.75	0.20172	0.1612	2.821	0.56
$h = \cos(\theta_o)$	0.3013	0.045238	0.07748	0.518	0.237
$2\mu(\text{Å}^{-1})$	1.846	0	3.161	0	0
R_{cut} (Å)	2.87 (2.95)[a]	2.2	3.1	2.9	3.1
D (Å)	0.15	0.2	0.2	0.2	0.2

[a] 2.95 is used for GaAs systems

Table 1: Parameter sets for the interactions.

4.4.1 Ga

Gallium has a complicated phase diagram with many stable and metastable structures close in energy to the ground state [50]. The stable low pressure phase α-Ga has seven nearest neighbours, six with the longer distance of "metallic" bonds and one near the dimer separation distance. At higher pressures Ga-II and Ga-III configurations with body-centered and face-centered tetragonal structures, respectively, are the stable configurations.

The potential reproduces the energetics and structural parameters of dimer, α-Ga, Ga-II, fcc-Ga and the hypothetical diamond and simple cubic structures. The parameters for the hypothetical structures were obtained by quantum mechanical methods. The bulk moduli for different structures is about 30 % lower than the experimental values or the values obtained by quantum mechanical calculations.

The cutoff parameters for the Ga-Ga interaction are different in papers II and III. The longer cutoff values have a melting point of 600±100 K. The shorter cutoff values in paper III lead to a higher melting point of 700±100 K. The shorter cutoff is needed to prevent the formation of long Ga-Ga bonds in wurtzite GaN. The melting points for both cutoff values are clearly higher than the experimental value 303 K [50], but not completely unreasonable considering that the potential describes the complex α-Ga structure. In the melting point simulations or subsequent melting and slow cooling simulations, gallium phases lower in energy than the α-Ga were not found.

4.4.2 As

The rhombohedral α phase occurring in the A7 structure is the stable phase of arsenic. The potential is fitted to reproduce the energetics and structural parameters of dimer, diamond, rhombohedral, simple cubic, bcc and fcc structures. The bulk moduli of different structures are in good agreement with experimental values.

The experimental melting point for As is 1090 K (determined at high pressures under As atmosphere [51]), which is lower than the boiling point, 880 K, determined at normal temperature and pressure. When arsenic liquid-solid equilibrium was simulated at 400 K, crystallization was observed. At 1200 K the whole system boiled, and intermediate behaviour was observed at temperatures of 700 K and 800 K. The melting properties of arsenic are therefore reasonably described by the model.

The rhombohedral α structure was the most stable structure found for the arsenic parametrization when simulating melting and slow cooling or the melting point. The relaxed structural parameter values for the α-As were in good agreement with the experimental and theoretical values.

4.4.3 N

Diatomic nitrogen has strong bonds, and N_2 has one of the highest binding energies of any molecule. A molecular crystal with weak van der Waals interactions between the dimers is formed at low pressures and temperatures. In recent experiments Eremets *et al.*[52] found evidence for a non-molecular structure of solid nitrogen forming at about 100 GPa.

Mailhiot *et al.*[53] have presented a theoretical study of the a stability of several crystalline structures of nitrogen based on DFT calculations. The fcc, sc, bcc and diamond structures were included in the fitting database of the Pauling relation. A slightly smaller dimer ground state oscillation frequency than the experimental one was chosen to allow a reasonable fit with the other structures. The final parameter set provides a very good fit to the calculated bond lengths and energies. The choice of a smaller ground state oscillation frequency of the dimer leads to higher bulk moduli for the other structures.

Many melting and subsequent cooling simulations were performed to search for artificial minima lying below the dimer molecule, but the dimer always appeared as the thermodynamically stable ground state.

4.4.4 GaAs

Zinc blende is the most stable structure for GaAs at low pressures and room temperature. At higher pressures orthorhombic GaAs-II, body-centered-orthorhombic GaAs-III and simple hexagonal GaAs-IV appear [54]. The energy-bond relation was fitted to the dimer, zinc blende, B1 and B2 structures. The B1 structure, which is fairly similar to the high pressure GaAs-II, was chosen to allow a better fitting of zinc blende properties. As a representative of highly coordinated structures, the metastable B2 phase was chosen, since none of the thermodynamically stable high pressure phases has a coordination of eight.

By choosing a dimer separation of 2.35 Å instead of the experimental value 2.53 Å , the structural properties of the solid phases can be described better. To get the correct elastic constants for the zinc blende structure, a ground state oscillation frequency of 278 cm^{-1}, which is still reasonably close to the experimental value 215 cm^{-1} [55], was selected.

The model gives a good description of elastic constants for zinc blende GaAs and is fitted to reproduce lattice parameters and cohesive energies of several structures with different coordinations. The melting point for the parameter set is 1900 ± 100 K, in good agreement with the experimental value of about 1500 K [56].

In another set of simulations, crystalline zinc blende GaAs was formed from an initially random set of atom coordinations. In these simulations the cell was cooled below the melting point of the potential model in one or more phases. The crystallization into zinc blende GaAs indicates that the zinc blende is the ground state structure of the potential model. Phases lower in energy to the zinc blende were not found in any of the simulations.

Defect formation energies for the potential model are in good agreement with DFT calculations, except for the As antisite, which has too high a formation energy. This may be related to the poor stability of the As-terminated structures described by the model. These two properties are strongly affected by the As-As parameters.

4.4.5 GaN

GaN is a highly ionic compound and the formalism used in this section can not describe the long range Coulombic interactions. A model explicitly including the long range interactions is presented and the effect of ionicity in GaN is discussed in section 4.5.

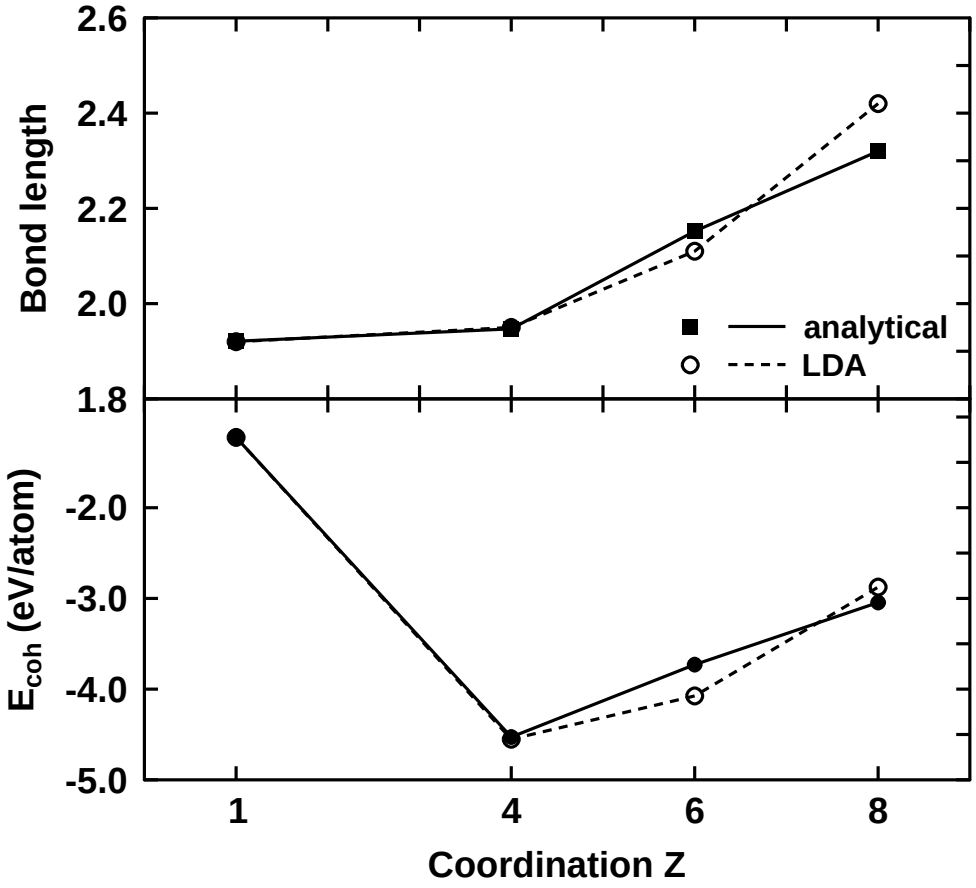

Figure 4: Cohesive energies and bond lengths for GaN dimer (Z=1), wurtzite (Z=4), B1 (Z=6) and B2 (Z=8) for the presented analytical model and the quantum mechanical LDA calculations.

The dimer properties of diatomic molecule GaN have been calculated by Kandalam *et al.*[57]. Since the dimer separation is longer than the second nearest neighbour distance of tetrahedrally bonded GaN, it can not be fitted with the present functional form. A shorter dimer bonding distance of 1.921 Å was therefore chosen. The calculated ground state oscillation frequency was also found to be too small to reproduce the elastic constants of solid GaN. Wurtzite, B1 (NaCl), B2 (CsCl) and dimer structures were used in the fit to the Pauling relation. The cohesive energies and bond lengths for the fitted structures are shown in Fig. 4.

To fit the elastic moduli, static elastic moduli for the zinc blende GaN were used. The hexagonal elastic moduli, the relaxed constants for zinc blende and the internal strain parameter were analyzed afterwards using the final parameter set. The results are in good agreement with experimental and theoretical values. Although the present model can not account for charge effects, the basic requirement for the defect properties was to reproduce the hierarchy in the formation energies of point defects. All other formation energies are accurately described except that of the Ga antisite, which has a formation energy that is significantly too small. The formation energies correspond to semi-insulating GaN. For

n-type GaN the formation energy of the gallium vacancy is smaller and the formation energy of the nitrogen vacancy is higher than in the present model. For p-type GaN the situation is reversed.

Extensive tests were carried out to ensure that the potential does not have states lower in energy than the correct ground state. Since the melting point for the potential model is 3500±500 K in good agreement with the experimental behaviour (experiments in a high-pressure cell showed that GaN does not melt at temperatures as high as 2753 K at 68 kbar [58]) and the solubility of atomic nitrogen in liquid gallium is described well by the parametrization, the potential can be used to model highly disordered phases.

4.5 Ionicity in GaN

The ionicity of GaN may significantly affect some of the processes involved in ion beam irradiation of the material. In the previous section a short ranged model for GaN is presented. Although the long range interactions are not explicitly included, the model reproduces many properties, that are important for the modeling of irradiation effects. To study the role of long range interactions on the high dose irradiation of GaN, a model explicitly including the Coulombic term is needed. In this section a long ranged model [59] is briefly described and results for the long and short range models are compared.

Since phase transitions occur during irradiation, a charge transfer model is needed. In the model described here, the local environment affects the charge distribution while charge neutrality is preserved.

In the model, every bond has a charge it can maximally transfer from one atom to another. The charge

$$\rho(r_{su}) = A\left(e^{-\frac{r_{su}-r_c}{\lambda}} - 1\right) \tag{14}$$

of the bond between atoms s and u depends on atom types through the parameter A. r_{su} is the distance between atoms s and u. r_c and λ are fitting parameters. The fraction of the charge that is transferred by the bond depends on the local neighborhood of atoms s and u. The weight factor P at the end of atom s is

$$P_{su} = \left(1 + \sum_{v \neq s,u} \frac{\rho(r_{sv})}{\rho(r_{su})}\right)^{-1/2n}. \tag{15}$$

The final charge state of the atom s is the sum of charges transferred by the bonds:

$$q_s = \sum_{u \neq s} \frac{P_{su} + P_{us}}{2} \rho(r_{su}). \tag{16}$$

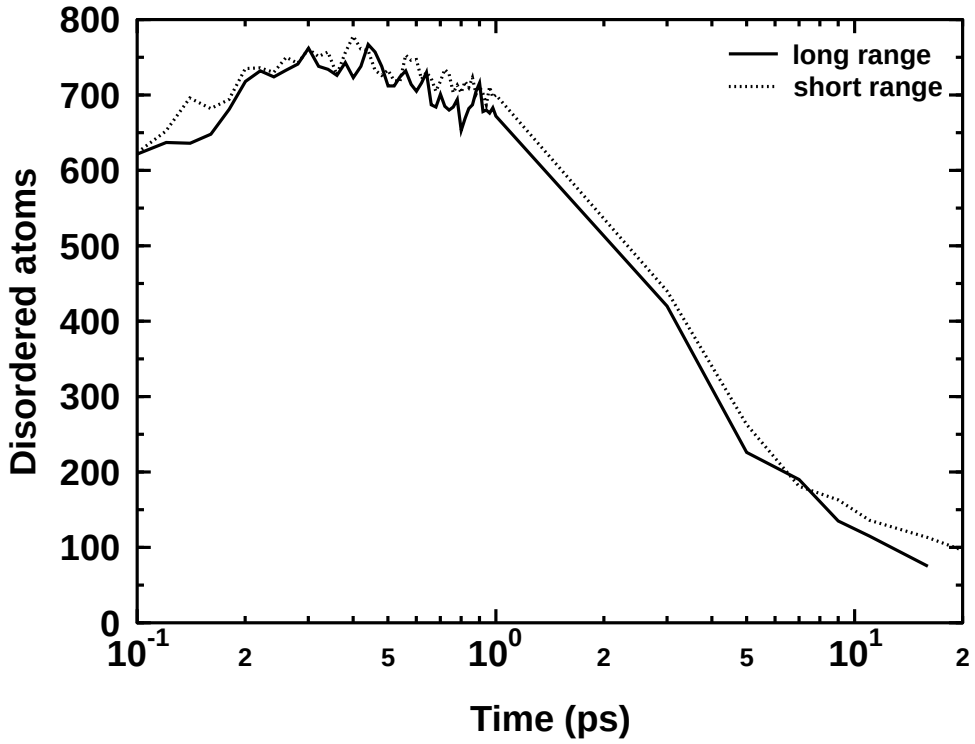

Figure 5: Number of disordered atoms vs. time after high energy density melt in crystalline GaN for long and short range potential models.

Here the effect of the neighborhood of atom u is transferred through P_{us}. The functional form also ensures charge neutrality. Covalent bonding is modeled by a functional form described in section 4.3 and the total energy is the sum of covalent and ionic terms:

$$E = \sum_i \sum_{j<i} f_{\mathrm{C}}(r_{ij})(V_{\mathrm{R}}(r_{ij}) - BijV_{\mathrm{A}}(r_{ij})) + \sum_i \sum_{j<i} \frac{q_i q_j}{4\pi\varepsilon_0 r_{ij}}. \quad (17)$$

The parameters in the charge model are fitted to charge data from quantum mechanical calculations for different structures. Since the difference between zinc blende and wurtzite GaN is caused by the difference in the Madelung sums of the structures, the energy contributions of covalent and charge terms can be calculated. About half of the potential energy of wurtzite GaN comes from the long range Coulombic interactions and another half from the covalent bonding. After the parameters for the charge part have been fitted, the covalent part is fitted to reproduce the elastic constants and energies of different structures.

To evaluate the effect of ionicity in the irradiation processes, individual cascades and recrystallization of liquid pockets were simulated using the long and short ranged models. The DPMTA algorithm [60] was used in the simulations to handle the long range forces efficiently.

Energy	Vacancies	Interstitials	Antisites
		Short range	
400 eV	2.8±0.4	2.8± 0.4	0.66± 0.2
1 keV	6.3±0.7	6.3± 0.7	2.1 ± 0.4
		Long range	
400 eV	3.0±1.2	3.0±1.2	0*
1 keV	6.3±1.1	6.3±1.1	3.3±0.3

*) Antisites were not observed in the five 400 eV simulations. More simulations are needed to obtain a more accurate number.

Table 2: Damage produced by 400 eV and 1 keV recoils with short and long range models. The number of defects is a sum of the defects in both Ga and N sublattices.

The defects produced in 400 eV and 1 keV cascades for both models are shown in table 2. Long and short range models predict very similar damage production in the recoil events.

To simulate the recrystallization of high energy density damage, a simulation cell consisting of 8192 atoms at perfect lattice sites was set up. The atoms closer than 10 Å to the center of the cell were given an initial velocity in random directions. The velocity was selected so that the cell heated up to about 2000 K after reaching thermal equilibrium. This way the center of the cell heated up quickly and produced a molten zone, which then partially recrystallized. The number of disordered atoms against time is given in Fig. 5 for the long and short range models. Again, the behaviour is fairly similar. A molten region of about 800 atoms is produced in the center of the cell. The disordered region quickly recrystallizes, and after 2 ps there are about 100 disordered atoms remaining. Slightly more recrystallization occurs with the ionic model and at long time scales the recombination might be more efficient with the long range model.

The results indicate that the covalent model can be used to model short timescale irradiation effects. Although the Coulombic interactions are not explicitly included in the model, they are implicitly taken into account at short length scales through the fitting of parameters to elastic constants and other properties.

5 MODELING OF HIGH DOSE IRRADIATION EFFECTS

Molecular dynamics simulations were used to model high dose irradiation effects in Si, Ge, GaAs and GaN. The simulation method is described in section 3.3. The results are published in papers IV-VI.

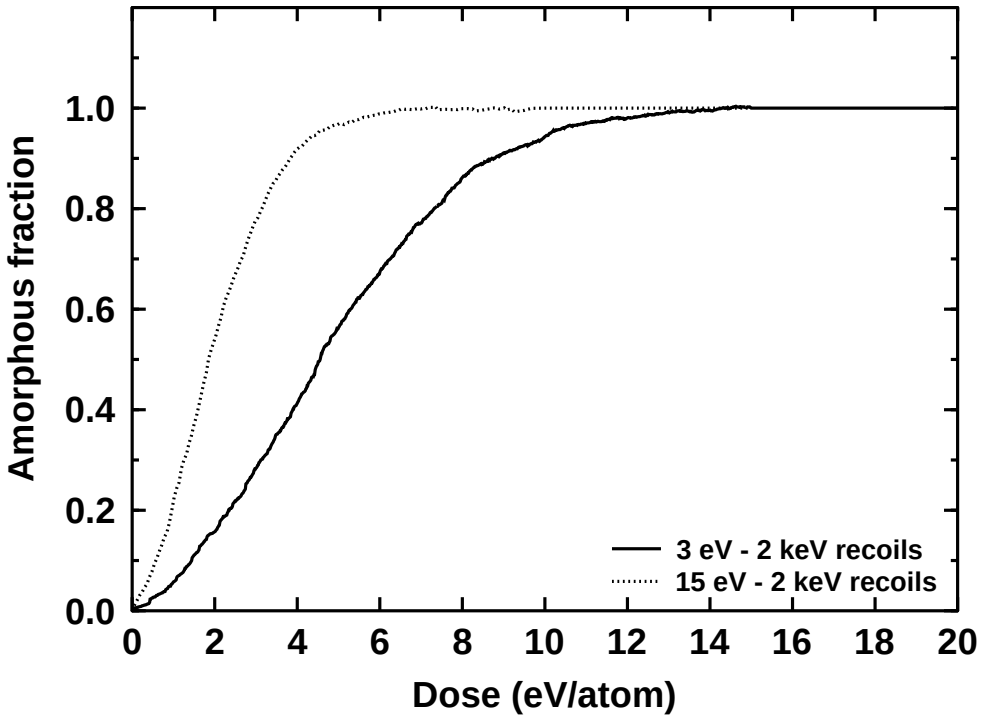

Figure 6: Amorphous fraction as a function of irradiation dose for 3 eV - 2 keV and 15 eV - 2 keV irradiated Si. Tersoff potential model was used in the simulations. A higher irradiation dose is needed to amorphize the material with 3-15 eV recoils included, because the low energy recoils cause recombination of defects.

5.1 Si

Three different interatomic potential models, Tersoff [29], Stillinger-Weber [34] and EDIP [31, 32], were used in modeling high dose irradiation of Si. The effects of pressure relaxation, random *vs.* simulated recoil angle distributions and different monoenergetic *vs.* simulated recoil energy distribution were analyzed.

The pressure was relaxed either in all three periodic directions or in one direction only. The one dimensional pressure relaxation corresponds to irradiation conditions, in which the sample prevents relaxation in the directions perpendicular to the beam. When the pressure was relaxed in only one direction, a higher dose was needed for the volume level to saturate. There were no structural differences in the final states, since the amorphous material flows slowly during prolonged irradiation.

Random and more realistic simulated angular distributions were used for recoil atoms. No differences were found between these conditions.

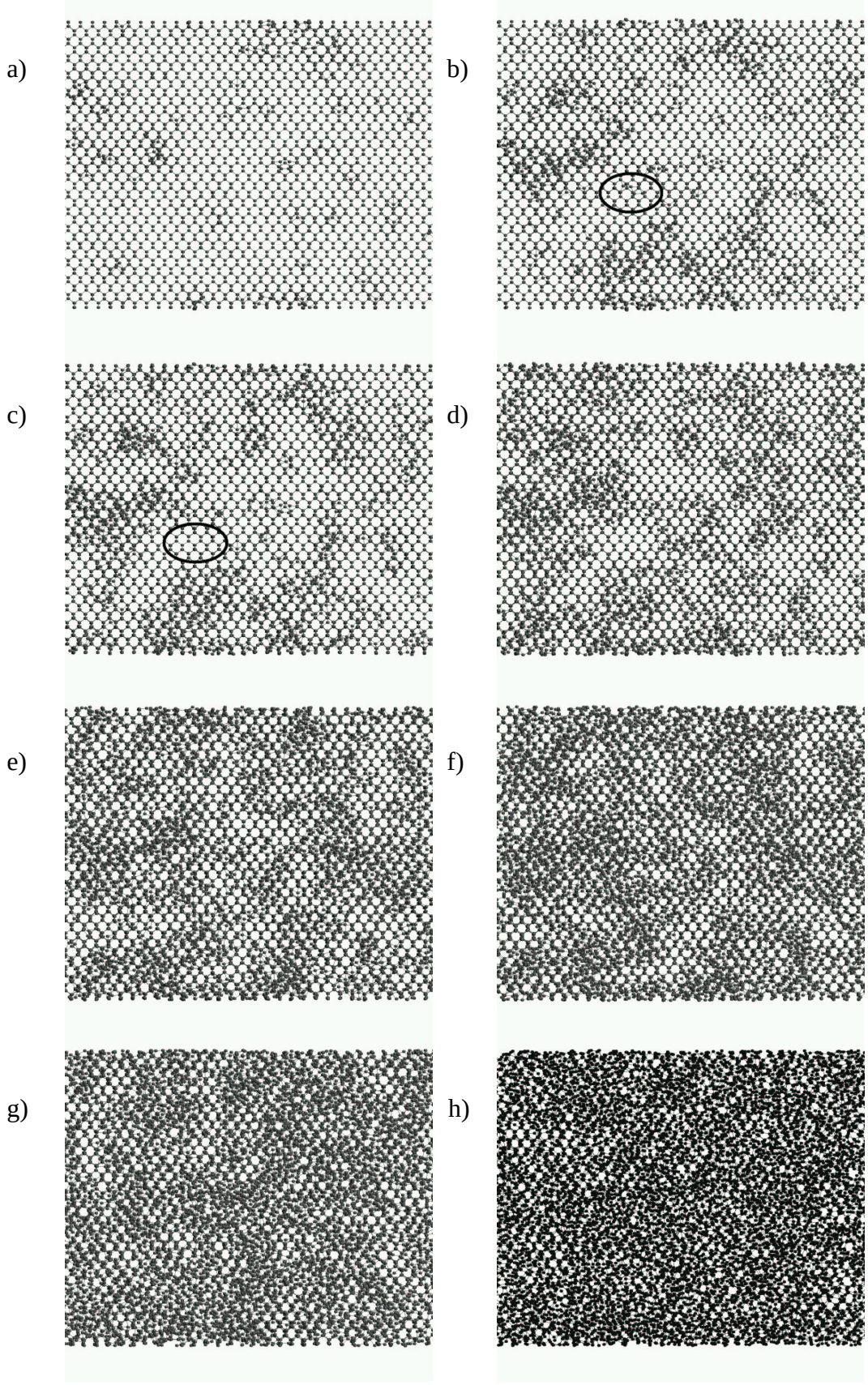

Figure 7: A 4 unit cell thick cross-section of the simulation cell during ion irradiation of Si. The doses are a) 0.3 eV/at. , b) 1.1 eV/at. , c) 1.4 eV/at. , d) 2.8 eV/at. , e) 4.3 eV/at. f) 5.7 eV/at, g) 7.1 eV/at. and h) 10.0 eV/at. An example of defect recombination is circled in b) and c). The T-III potential model and simulated recoil energy distribution with 3 eV minimum recoil energy were used.

Several different recoil energy distributions were used. Two distributions consisted of only one energy, either 100 eV or 1 keV. A more realistic recoil energy distribution was simulated using MDRANGE [23]. Either 3 eV or 15 eV lower energy and 2 keV higher energy cutoffs were used. It was found that when using 1 keV recoils the volume and potential energy changes were smaller than for other conditions, because localized heating can recombine defects more efficiently in this case. The amorphization process is illustrated in Fig. 7. Comparing the results with the 3 eV low energy cutoff to the other results, it was observed that the low energy recoils (3 - 15 eV) can cause significant athermal recrystallization during irradiation. The difference in the development of amorphous fraction is illustrated in Fig. 6.

The volume development during irradiation was different for the three potential models. For the Tersoff and EDIP potentials the volume change was positive in agreement with experiments (irradiated at 77 K temperature [61]), whereas for SW the change was negative. For all the potential models the average potential energy was higher for the irradiated amorphous structure than for the quenched one, which shows that defects are present in the irradiated amorphous structure. The average bond length was longer and the average coordination number higher for the irradiated amorphous cell than for the quenched amorphous structure. The doses needed to amorphize Si were in good agreement with experiments performed at 77 K.

Both the Tersoff and EDIP potentials generate structures whose pair correlation functions agree well with the experimental measurements. The SW model has an additional peak at 3 Å , which is not observed in the experiments. Since the SW potential also predicts a negative volume change, it is concluded that the SW gives a poorer description of the high dose irradiation process than the other two models used here.

The annealing simulations showed that after annealing the irradiated cells collapse into structures similar to the quenched ones.

5.2 Ge

For Ge, Stillinger-Weber [34, 35] and Tersoff [33] potential models were used. The amorphization was simulated by using successive 1 keV recoils. As in the case of Si, both models predict longer bonds for the irradiated than for the quenched or crystalline structures. Both models also predict a higher coordination for the amorphous than for the crystalline structure.

For the Tersoff potential model the density decreases in the beginning of the amorphization process and then increases to about the level of crystalline Ge. For SW, the volume grows monotonically throughout the simulation.

The Stillinger-Weber model predicts a small increase in the coordination number, which agrees well with experimental [62] and *ab – initio* values [63]. It also produces a pair correlation function, which is in good agreement with experiments. The Tersoff potential predicts too strong a change in the coordination number, but the pair-correlation function is well reproduced.

The amorphization dose for the Tersoff model was in good agreement with experiments (at 77 K temperature). The SW model had too high an amorphization dose probably because it overestimates the melting point of Ge.

5.3 GaAs

Only one potential model was used for GaAs due to the lack of interatomic potential models that are able to describe pure Ga and As structures. The model is presented in paper II.

Successive 1 keV recoils were used to model the amorphization. The amorphization dose was about 13 eV/atom, which is in reasonable agreement with the experimental value of about 10 eV/atom (implanted at 80 K, see paper II). The volume of the cell increased by about 4.5 %, which was reduced to about 2.9 % after annealing. The change is in good agreement with the experimental value of about 4% [64].

After amorphization, the fraction of like-atom covalent bonds was about 14 %, which is more than was observed in the experiments (0-12 %, see references in paper II). The average coordination number was between 3.45 and 4.64 depending on whether the weak Ga-Ga bonds were counted. The coordination number of less than 4 for covalent bonds and the increase in bond length agree with the experimental observation [64].

During a 400 ps annealing of the amorphized cell at 900 K, the number of Ga-Ga bonds decreased by about 13 %, indicating that the bonds are not stable at high temperatures. Although the number of As-As bonds was increased, longer simulation starting from random positions of atoms have shown that pure As zones decrease in size in longer time scales. The annealing also decreased the length difference between like atom bonds and Ga-As bonds.

The simulation produces at least qualitatively some properties of the amorphous GaAs (density change, a coordination number of less than 4 and the presence of the wrong bonds). The change

of the properties was larger in our simulation than in the experiments, which may be due to long-term annealing effects not described by the MD model.

5.4 GaN

GaN is more difficult to amorphize than Si, Ge or GaAs and complex amorphization behavior has been observed during irradiation [65, 66]. To study the processes involved, molecular dynamics methods can be an effective tool.

High dose irradiation was modeled by using the potential model presented in paper III and section 4. The model does not include long range Coulombic interaction, but as discussed in section 4.5 this does not seem to be a problem in irradiation simulations.

Both individual cascades and high dose irradiation by successive 400 eV or 5 keV recoils were simulated. For individual ions the incidence angle dependence of the damage was studied at the surface.

The simulations show that much less damage is produced by the individual recoils in GaN than in GaAs. This explains much of why the irradiation dose required to amorphize GaN is much higher than that in GaAs. Another factor is the dynamic annealing, in which local heating causes the recombination of defects. The effect is related to a dip in the damage production, which is observed above a recoil energy of 1 keV for individual ions. A similar effect was observed in the recrystallization simulations presented in section 4.5, but in the case of collision cascades the effect is smaller because the energy is more scattered.

Five keV Er ions were bombarded at perfect wurtzite GaN to study the effects of incidence angle on the damage production. The total number of interstitials and the number of interstitials in clusters compared to the experimentally observed damage level are shown in Fig. 8. Qualitatively, the results from the different measures of damage behave the same way; the damage is increased as the implantation angle is increased from 5 to 10 degrees, but is almost constant for smaller angles. However, the increase in the total number of interstitials is smaller than the experimentally observed increase in damage level. The number of interstitials in clusters agrees very well with the experimentally observed behavior. It is therefore concluded that the experimental damage production is explained by direct impact amorphous pockets and that the mobile point defects recombine and therefore give no contribution to the measured defect density.

The high dose irradiation of GaN was studied by simulating successive 400 eV and 5 keV recoils. The amorphization dose was about 40 eV/atom for both recoil energies, but the damage saturated at a

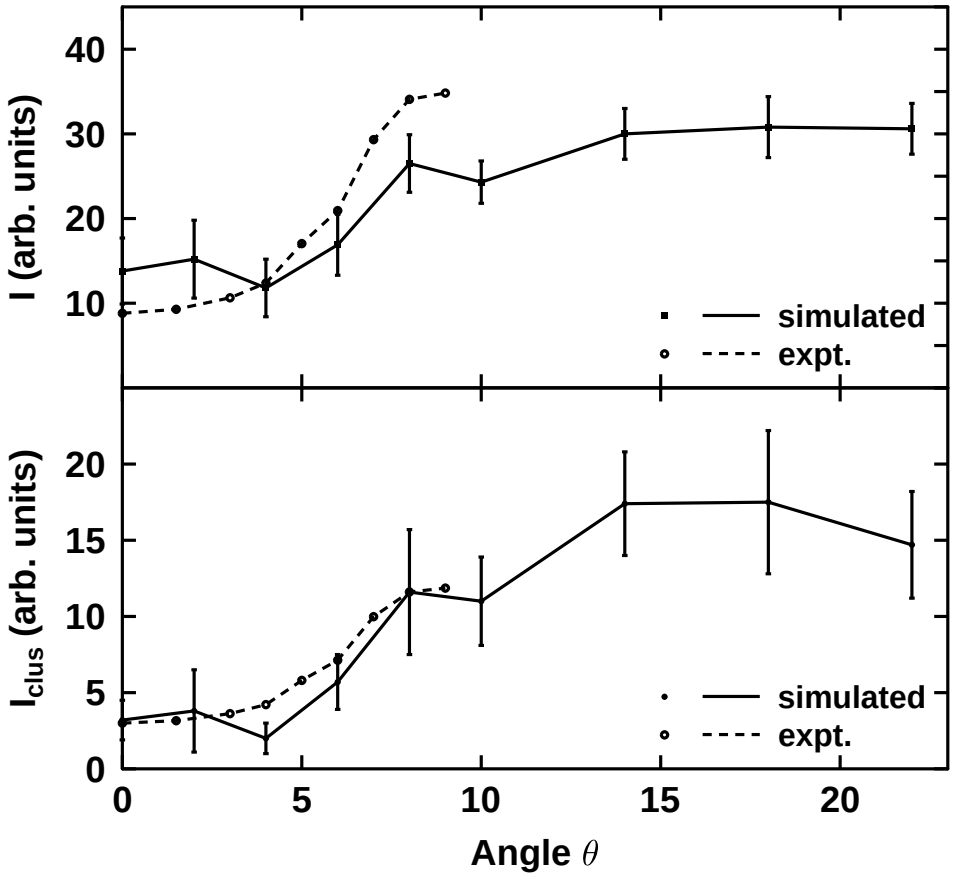

Figure 8: Comparison between the experimental defect density [67] and the total number of interstitials (upper figure) and the number of interstitials in clusters (lower figure) in Er doped GaN as a function of implantation angle. The amount of damage in clusters describes the experimentally observed behavior better than the total number of interstitials.

lower level for the 5 keV case. Since heavy ions produce more high energy recoils, this may explain the variation in the saturation level observed in experiments for different heavy ions [65].

Amorphization proceeded in the simulations as follows. Highly separate defects were formed during the early stages of the irradiation, which caused the wurtzite lattice to distort. Long Ga-Ga bonds were formed in the distorted lattice. During the process, N_2 gas was formed, but regions with only gallium atoms were not observed. In the high damage region, local heating started to cause the recombination of defects for high energy recoils.

Although the dose needed to amorphize the material is much higher than that for Si, Ge and GaAs, it is still lower than the experimental value (about 90 eV/atom at 120 K [68]). Since the simulation can not fully explain the high amorphization dose for GaN, it is likely that in addition to the observed effects, there are long time scale and long range processes which our model can not handle.

6 CONCLUSIONS

This thesis deals with the damage produced during high dose implantation in Si, Ge, GaAs and GaN. Molecular dynamics methods are used in the modeling.

The quality of the present interatomic potential models is estimated and new models are developed for GaAs and GaN. The role of ionicity in the short time scale processes of damage production during ion beam irradiation of GaN is examined.

Comparison of the experimental and simulated results of high dose irradiation in Si, Ge, GaAs and GaN has produced information about the mechanisms leading to amorphization, important factors in the process, the structure of the amorphous material and the interatomic potential models used in the simulations.

It was found that the low energy (3 - 15 eV) recoils can cause significant athermal recrystallization during irradiation in Si. For GaN, two reasons were found for the high amorphization dose: the high threshold displacement energy leading to low damage production in individual cascades and in-cascade recombination of defects. The simulations showed that the angular dependence of the damage during Er bombardment of GaN can be understood by the direct impact amorphous pockets.

ACKNOWLEDGMENTS

I wish to thank the former and current heads of the laboratory, Doc. Eero Rauhala and Prof. Jyrki Räisänen for providing the facilities of the laboratory for my disposal. I thank Prof. Juhani Keinonen, the head of the Department of Physical Sciences, for the opportunity to conduct research at the department and for his advice during this work.

Special thanks are due to Prof. Kai Nordlund for introducing the wondrous worlds of materials science and molecular dynamics to me. All colleagues and co-authors at the laboratory and outside world are acknowledged for providing valuable discussions and entertaining events.

Warm thanks to Aleksanteri and Suvi for being part of my life.

Financial support from the Academy of Finland, and the Väisälä and Magnus Ehrnrooth foundations is gratefully acknowledged.

Helsinki, August 2003
Janne Nord

REFERENCES

1. *International Technology Roadmap for Semiconductors*, 2002 update, published by the Semiconductor Industry Association (SIA).

2. E. Chason, S. T. Picraux, M. Poate, J. O. Borland, M. I. Current, T. Diaz de la Rubia, D. J. Eaglesham, O. W. Holland, M. E. Law, C. W. Magee, J. W. Mayer, J. Melngailis, and A. F. Tasch, *Ion beams in silicon processing and characterization*, J. Appl. Phys **81**, 6513 (1997).

3. S. C. Jain, M. Willander, J. Narayan, and R. V. Overstraeten, *III-Nitrides: Growth, characterization, and properties*, Appl. Phys. Lett. **87**, 965 (2000).

4. J. R. Dennis and E. B. Hale, *Crystalline to amorphous transformation in ion-implanted silicon: a composite model*, J. Appl. Phys. **49**, 1119 (1978).

5. N. Hecking, K. F. Heidemann, and E. T. Kaat, *Model of temperature dependent defect interaction and amorphization in crystalline silicon during ion irradiation*, Nucl. Instr. Meth. Phys. Res. B 760 (1986).

6. G. Bai and M. A. Nicolet, *Defects production and annealing in self-implanted Si*, J. Appl. Phys. **70**, 649 (1991).

7. G. Carter, *The effects of flux, fluence and temperature on amorphization in ion implanted semiconductors*, J. Appl. Phys. **11**, 8285 (1996).

8. W. J. Weber, *Models and mechanisms of irradiation-induced amorphization in ceramics*, Nucl. Instr. Meth. Phys. Res. B **166-167**, (2000), 98-106.

9. S. X. Wang, L. M. Wang, and R. C. Ewing, *Irradiation-induced amorphization: Effects of temperature, ion mass, cascade size, and dose rate*, Phys. Rev. B **63**, 024105 (2000).

10. M. T. Robinson and I. M. Torrens, *Computer Simulation of atomic-displacement cascades in solids in the binary-collision approximation*, Phys. Rev. B **9**, 5008 (1974).

11. L. Pelaz, L. A. Marques, M. Aboy, G. Gilmer, L. A. Bailon, and J. Barbolla, *Monte Carlo modeling of amorphization resulting from ion implantation in Si*, Comp. Mat. Sci. **27**, 1 (2003).

12. L. Pelaz, L. A. Marques, M. Aboy, and J. Barbolla, *Atomistic modeling of amorphization and recrystallization in silicon*, Appl. Phys. Lett. **82**, 2038 (2003).

13. G. Lulli, E. Albertazzi, M. Bianconi, R. Nipoti, M. Cervera, A. Carnera, and C. Cellini, *Stopping and damage parameters for Monte Carlo simulation of MeV implants in crystalline Si*, J. Appl. Phys. **82**, 5958 (1997).

14. J. M. Hernandez-Mangas, J. Arias, L. Bailon, M. Jaraiz, and J. Barbolla, *Improved binary collision approximation ion implant simulators*, J. Appl. Phys. **91**, 658 (2002).

15. S. Tian, *Predictive Monte Carlo ion implantation simulator from sub-keV to above 10 MeV*, J. Appl. Phys. **93**, 5893 (2003).

16. M. J. Caturla, T. D. de la Rubia, and G. H. Gilmer, *Recrystallization of a planar amorphous-crystalline interface in silicon by low energy recoils: A molecular dynamics study*, J. Appl. Phys. **77**, 3121 (1995).

17. D. M. Stock, G. H. Gilmer, M. Jaraiz, and T. D. de la Rubia, *Point defect accumulation in silicon irradiated by energetic particles: A molecular dynamics study*, Nucl. Instr. Meth. Phys. Res. B **102**, 207 (1995).

18. B. Weber, K. Gärtner, and D. M. Stock, *MD-simulation of ion induced crystallization and amorphization processes in silicon*, Nucl. Instr. Meth. Phys. Res. B **127/128**, 239 (1997).

19. K. M. Beardmore and N. Grønbech-Jensen, *Direct simulation of ion-beam-induced stressing and amorphization of silicon*, Phys. Rev. B **60**, 12610 (1999).

20. F. Gao and W. J. Weber, *Cascade overlap and amorphization in 3C-SiC: Defect accumulation, topological features, and disordering*, Phys. Rev. B **66**, 024106 (2002).

21. F. Gao, W. J. Weber, and R. Devanathan, *Defect production, multiple ion-solid interactions and amorphization in SiC*, Nucl. Instr. Meth. Phys. Res. B **191**, 487 (2002).

22. H. J. C. Berendsen, J. P. M. Postma, W. F. van Gunsteren, A. DiNola, and J. R. Haak, *Molecular dynamics with coupling to external bath*, J. Chem. Phys. **81**, 3684 (1984).

23. K. Nordlund, *Molecular dynamics simulation of ion ranges in the 1 – 100 keV energy range*, Comput. Mater. Sci. **3**, 448 (1995).

24. D. W. Brenner, *Relation between the Embedded-Atom method and Tersoff potentials*, Phys. Rev. Lett. **63**, 1022 (1989).

25. B. J. Thijsse, *Relationship between the modified embedded-atom method and Stillinger-Weber potentials in calculating the structure of silicon*, Phys. Rev. B **65**, 195207 (2002).

26. N. Mousseau and L. J. Lewis, *Topology of amorphous Tetrahedral semiconductors on intermediate length scales*, Phys. Rev. Lett. **78**, 1484 (1997).

27. H. Balamane, T. Halicioglu, and W. A. Tiller, *Comparative study of silicon empirical interatomic potentials*, Phys. Rev. B **46**, 2250 (1992).

28. J. Tersoff, *Empirical interatomic potential for silicon with improved elastic properties*, Phys. Rev. B **38**, 9902 (1988).

29. J. Tersoff, *New empirical approach for the structure and energy of covalent systems*, Phys. Rev. B **37**, 6991 (1988).

30. F. H. Stillinger and T. A. Weber, *Computer simulation of local order in condensed phases of silicon*, Phys. Rev. B **31**, 5262 (1985).

31. M. Z. Bazant and E. Kaxiras, *Environment-dependent interatomic potential for bulk silicon*, Phys. Rev. B **56**, 8542 (1997).

32. J. F. Justo, M. Bazant, E. Kaxiras, V. V. Bulatov, and S. Yip, *Interatomic potential model for silicon defects and disordered phases*, Phys. Rev. B **58**, 2539 (1998).

33. J. Tersoff, *Modeling solid-state chemistry: Interatomic potentials for multicomponenet systems*, Phys. Rev. B **39**, 5566 (1989).

34. K. Ding and H. C. Andersen, *Molecular-dynamics simulation of amorphous germanium*, Phys. Rev. B **34**, 6987 (1986).

35. K. Nordlund, M. Ghaly, R. S. Averback, M. Caturla, T. Diaz de la Rubia, and J. Tarus, *Defect production in collision cascades in elemental semiconductors and FCC metals*, Phys. Rev. B **57**, 7556 (1998).

36. R. Smith, *A semi-empirical many-body interatomic potential for modlling dynamical processes in gallium arsenide*, Nucl. Instr. Meth. Phys. Res. B 335 (1992).

37. M. Sayed, J. H. Jefferson, A. B. Walker, and A. G. Cullis, *Molecular dynamics simulations of implantation damage and recovery in semiconductors*, Nucl. Instr. Meth. Phys. Res. B **102**, 218 (1996).

38. K. Nordlund and A. Kuronen, *Non-equilibrium properties of GaAs interatomic potentials*, Nucl. Instr. Meth. Phys. Res. B **159**, 183 (1999).

39. T. Ito, K. E. Khor, and S. D. Sarma, *Systematic approach to developing empirical potentials for compound semiconductors*, Phys. Rev. B **41**, 3893 (1990).

40. M. Ichimura, *Stillinger-Weber potentials for III-V compound semiconductors and their application to the critical thickness calculation for InAs/GaAs*, Phys. Stat. Sol. **153**, 431 (1996).

41. D. Conrad and K. Scheerschmidt, *Empirical bond-order potential for semiconductors*, Phys. Rev. B **58**, 4538 (1998).

42. P. Zapol, R. Pandey, and J. Gale, *An interatomic potential study of the properties of gallium nitride*, J. Phys.: Condens. Matter **9**, 9517 (1997).

43. S. Wang, Y. Wang, and H. Ye, *A theoretical study on various models for the domain boundaries in epitaxial GaN films*, Appl. Phys. A (70).

44. N. Aïchoune, V. Potin, P. Rutena, A. Hairie, G. Nouet, and E. Paumier, *An empirical potential for the calculation of the atomic structure of extended defects in wurtzite GaN*, Comp. Mat. Sci. **17**, 380 (2000).

45. D. W. Brenner, *The art and science of an analytic potential*, Phys. stat. sol (b) **217**, 23 (2000).

46. G. C. Abell, *Empirical chemical pseudopotential theory of molecular and metallic bonding*, Phys. Rev. B **31**, 6184 (1985).

47. K. Albe, K. Nordlund, and R. S. Averback, *Modeling metal-semiconductor interaction: Analytical bond-order potential for platinum-carbon*, Phys. Rev. B **65**, 195124 (2002).

48. W. H. Press, S. A. Teukolsky, W. T. Vetterling, and B. P. Flannery, *Numerical Recipes in C; The Art of Scientific Computing*, 2nd ed. (Cambridge University Press, New York, 1995).

49. J. R. Morris, C. Z. Wang, K. M. Ho, and C. T. Chan, *Melting line of aluminum from simulations of coexisting phases*, Phys. Rev. B **49**, 3109 (1994).

50. L. Bosio, *Crystal structures of Ga(II) and GA(III)*, J. Chem. Phys. **68**, 1221 (1978).

51. R. Bellissent, C. Bergman, R. Ceolin, and J. Gaspard, *Structure of Liquid As: A Peierls Distortion in a liquid*, Phys. Rev. Lett. **59**, 661 (1987).

52. M. I. Eremets, R. Hemley, H. Mao, and E. Gregoryanz, *Semiconducting non-molecular nitrogen up to 240 GPa and its low-pressure stability*, **411**, 170 (2001).

53. C. Mailhiot, L. H. Yang, and A. K. McMahan, *Polymeric nitrogen*, Phys. Rev. B **46**, 14419 (1992).

54. M. McMahon and R. Nelmes, *Observation of a cinnabar phase in GaAs at high pressure*, Phys. Rev. Lett. **78**, 3697 (1997).

55. G. Lemire, G. Bishea, S. Heidecke, and M. Morse, *Spectroscopy and electronic structure of jet-cooled GaAs*, J. Chem. Phys. **92**, 121 (1990).

56. J. A. V. Vechten, *Quantum Dielectric Theory of Electronegativity in Covalent Systems. III. Pressure-Temperature Phase Diagrams, Heats of Mixing, and Distribution Coefficients*, Phys. Rev. B **7**, 1479 (1973).

57. A. Kandalam, R. Pandey, M. Blanco, A. Costales, J. Recio, and J. Newsam, *First Principles study of polyatomic clusters of AlN, GaN and InN. 1. Structure, Stability, Vibrations and Ionization*, J. Phys. Chem. B **104**, 4361 (2000).

58. *Properties of group III nitrides*, edited by J. Edgar (INSPEC, London, 1994).

59. K. Albe, K. Nordlund, and J. Nord, to be published.

60. W. T. Rankin and J. J. A. Board, *Proceedings of the 1995 IEEE Symposium on High Performance Distributed Computing* (IEEE Computer Society Press, Los Alamitos, California, 1995), pp. 17–22, ; W. T. Rankin, PhD Thesis, Duke University, 1995.

61. J. S. Custer, M. O. Thompson, D. C. Jacobson, J. M. Poate, S. Roorda, W. C. Sinke, and F. Spaepen, *Density of amorphous Si*, Appl. Phys. Lett. **64**, 437 (1994).

62. M. C. Ridgway and C. J. Glover, *Ion-dose-dependent microstructure in amorphous Ge*, Phys. Rev. B **61**, 12586 (2000).

63. G. Kresse and J. Hafner, *Ab initio molecular-dynamics simulation of the liquid-metal-amorphous-semiconductor transition in germanium*, Phys. Rev. B **49**, 14251 (1994).

64. M. C. Ridgway, C. J. Glover, G. J. Foran, and K. M. Yu, *Characterization of the local structure of amorophous GaAs produced by ion implantation*, J. Appl. Phys. **83**, 4610 (1998).

65. S. O. Kucheyev, J. S. Williams, and C. Jagadish, *Effect of ion species on the accumulation of ion-beam damage in GaN*, Phys. Rev. B **64**, 035202 (2001).

66. E. Wendler, A. Kamarou, E. Alves, K. Gärtner, and W. Wesch, *Three-step amorphization process in ion-implanted GaN at 15 K*, Nucl. Instr. Meth. Phys. Res. B , in press.

67. B. Pipeleers, S. M. Hogg, and A. Vantomme, to be published.

68. C. Liu, A. Wenzel, B. Rauschenbach, E. Alves, A. D. Sequira, N. Franco, M. F. da Silva, J. C. Soares, and X. J. FaN, *Amorphization of GaN by ion implantation*, Nucl. Instr. Meth. Phys. Res. B **178**, 200 (2001).